 doi:10.20944/preprints202104.0346.v1

Article

A Real-Time Circuit Phase Delay Correction System for MEMS Vibratory Gyroscopes

Pengfei Xu [1,2], Zhenyu Wei [1,2], Zhiyu Guo [1,2], Lu Jia[1,2], Guowei Han [1,*], Chaowei Si [1,*], Jin Ning [1,3,4], and Fuhua Yang [1,2,*]

[1] Engineering Research Center for Semiconductor Integrated Technology, Institute of Semiconductors, Chinese Academy of Sciences, Beijing 100083, China; xupengfei@semi.ac.cn (P.X.); zywei97@semi.ac.cn (Z.W.); gzy@semi.ac.cn (Z.G.); jialu@semi.ac.cn (L.J.); ningjin@semi.ac.cn (J.N.);
[2] College of Materials Science and Opto-Electronic Technology, University of Chinese Academy of Sciences, Beijing 100049, China
[3] School of Electronic, Electrical and Communication Engineering, University of Chinese Academy of Sciences, Beijing 100049, China
[4] State Key Laboratory of Transducer Technology, Chinese Academy of Sciences, Beijing 100083, China
* Correspondence: hangw1984@semi.ac.cn (G.H.); schw@semi.ac.cn (C.S.); fhyang@semi.ac.cn (F.Y.); Tel.: +86-10-8230-5403 (G.H.)

Abstract: With the development of designing and manufacturing level for micro-electromechanical system (MEMS) gyroscopes, the control circuit system becomes a key point to determine their internal performances. Nevertheless, phase delay of electron components may result in some serious hazards. This paper describes a real-time circuit phase delay correction system for MEMS vibratory gyroscopes. A detailed theoretical analysis is provided to clarify the influences of circuit phase delay on the in-phase and quadrature (IQ) coupling characteristics and zero rate output (ZRO) utilizing force-to-rebalance (FTR) closed-loop detection and quadrature correction system. By deducing the relationship between amplitude-frequency, phase-frequency of MEMS gyroscope and the phase relationship of the whole control loop, a real-time correction system is proposed to automatically adjust the phase reference value of phase-locked loop (PLL) and thus compensate for the real-time circuit phase delay. The experimental results show that the correction system can accurately measure and compensate the circuit phase delay in real time. Furthermore, the unwanted IQ coupling can be eliminated and the ZRO is decreased by 755% to 0.095°/s. This correction system realizes a small angle random walk of 0.978°/√h, and a low bias instability of 9.458°/h together with a scale factor nonlinearity of 255 ppm at room temperature. Besides, the thermal drift of ZRO is reduced to 0.0034°/s/°C at a temperature range from -20°C to 70°C.

Keywords: MEMS gyroscopes; circuit phase delay; IQ coupling; real-time correction system

1. Introduction

Micro-electromechanical system (MEMS) gyroscopes, measuring the angular rate motion based on the Coriolis effect [1], has been widely adopted for industrial and consumer applications [2,3] for its small size, high integration, low cost and low power consumption. With the rapid development of electronic techniques, the performance of MEMS gyroscopes has been considerably improved, bringing a new future for potential military applications [4-7].

Vibratory gyroscopes work through Coriolis coupling between two orthogonal modes where one mode is forced to oscillate along the drive axis while the other operates as an accelerometer sensing the angular rate-induced Coriolis acceleration along the sense axis [8,9]. Limited by the manufacturing imperfections and immature packaging techniques, in-phase and quadrature error, caused by damping and stiffness coupling, are inevitable for vibratory gyroscopes [10]. Theoretically, the desired angular rate and unwanted quadrature error signals are orthogonal and could be separated via a phase-sensitive demodulation method because they are respectively

modulated by the drive velocity and displacement [11]. However, the gyroscope can not work in the resonant state when circuit phase delay (generated by ADC, DAC, C/V, and etc.) exists. In this case, the quadrature error is not -90° out of phase with the angular rate signal, introducing a skew between the quadrature and in-phase channel and hence causing in-phase and quadrature (IQ) coupling [12,13].

The existence of quadrature errors seriously affects the performances of gyroscopes, especially the dynamic range, bias stability and temperature sensitivity [14,15]. To eliminate the unwanted quadrature error signals, quadrature cancellation technique is widely used in the closed-loop control electronics to improve bias instability (BI), angle random walk (ARW), the linearity of the scale factor and the dynamic range of the interface circuit [16-18]. However, this technique is sensitive to phase error for these two channels. Besides, its effectiveness is greatly limited by the stability and accuracy of the phase relationship between the demodulation and the sense signal [19,20]. It was proved that open-loop detection and different phase compensation methods can effectively compensate the errors caused by circuit phase delay, but they are inapplicable to most gyroscope control circuits [11,12]. A one-time off-line frequency sweep procedure was proposed to eliminate the in-phase Coriolis and the quadrature signal [21], and the circuit phase delay was compensated by modifying the reference value of the phase-locked loop (PLL). Nevertheless, this method cannot always accurately reflect the true circuit phase delay. A novel procedure, force-to-rebalance (FTR) control, is used to calculate the total phase delay within the working process by adopting a digital all-pass filter to realize one-time phase self-compensation [13]. It should be noted that no real-time phase delay correction method has been mentioned until now, and further researches are in crying needs to realize real-time circuit phase delay correction in order to improve the performance of MEMS gyroscopes.

In this work, we demonstrate a real-time circuit phase delay correction system to compensate the unwanted circuit phase delay for MEMS vibratory gyroscopes. The influence of circuit phase delay on the IQ coupling characteristics and zero rate output (ZRO) is analyzed via FTR closed-loop detection and quadrature correction system. Meanwhile, a detailed theoretical analysis for the effect of circuit phase delay on the in-phase and quadrature channels is given. Based on the amplitude-frequency, phase-frequency characteristics of MEMS gyroscopes and phase relationship of the whole control loop, we design a correction system to automatically measure and compensate the real-time circuit phase delay. This goal is achieved by collecting the amplitude of automatic gain control (AGC) excitation signal and then automatically adjusting the phase reference value of the PLL. It is shown that this correction system is robust against the temperature change, and the compensated circuit phase delay is the true phase delay in the working process. Notably, we, for the first time, propose a real-time circuit phase delay correction system which can accurately measure and compensate the circuit phase delay in real time to effectively eliminate the unwanted IQ coupling and reduce the effect of quadrature error on ZRO, dramatically improving the BI and ARW performance of gyroscope.

2. MEMS Gyroscope Dynamic Overview

A simplified model of a z-axis MEMS vibratory gyroscope is shown in Fig. 1. Where x-axis, y-axis, and z-axis is the drive, the sense, and the angular velocity input direction, respectively [22]. The c, k, and m_c represent the damping coefficient, stiffness coefficient, and the mode mass. A MEMS vibratory gyroscope is composed of two orthogonal mechanical resonators, called the drive mode and the sense mode, which can be described as a mass-damper-spring second-order system.

Preprints (www.preprints.org) | NOT PEER-REVIEWED | Posted: 13 April 2021 doi:10.20944/preprints202104.0346.v1

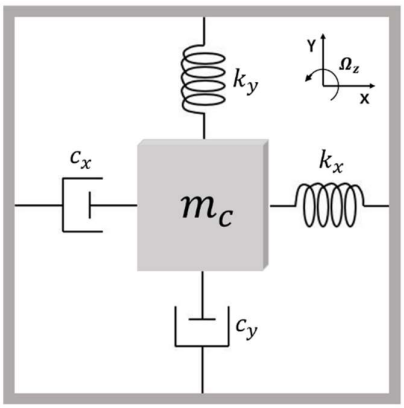

Figure 1. A simplified model of MEMS vibratory gyroscope

Ideally, the simplified dynamic equations of the vibrating gyroscope are revealed in Equation (1) and (2):

$$m_x\ddot{x} + c_x\dot{x} + k_x x = F_x(t) \tag{1}$$

$$m_y\ddot{y} + c_y\dot{y} + k_y y = F_y(t) - 2m_C\Omega_z\dot{x} \tag{2}$$

where m_x and m_y represent the effective mass in x and y direction respectively, which are equal to Coriolis mass m_C, Ω_z is the angular velocity input, $F_x(t) = A_f \cos(w_d t)$ is the drive force (A_f is the excitation amplitude and w_d is the drive force frequency), $F_y(t)$ is the sense force (i.e. $F_y(t) = 0$, when the sense mode is under open-loop). The expression of drive resonant frequency w_x and drive quality factor Q_x are:

$$w_x = \sqrt{\frac{k_x}{m_x}} \tag{3}$$

$$Q_x = \frac{m_x w_x}{c_x} \tag{4}$$

Substituting Equation (3) and (4) into (1) yields, the transient-response $x(t)$ of the mass in the drive direction can be obtained:

$$x(t) = A_x cos(w_d t + \varphi_x) \tag{5}$$

$$|A_x| = \frac{A_f/m_x}{\sqrt{(w_x^2 - w_d^2)^2 + w_x^2 w_d^2/Q_x^2}} \tag{6}$$

$$\varphi_x = -arctan\frac{w_x w_d}{Q_x(w_x^2 - w_d^2)} \tag{7}$$

where $|A_x|$ is the amplitude of the vibration displacement, φ_x is the drive phase delay, when the drive force frequency w_d is accurately locked to the drive resonant frequency w_x by PLL, the vibration amplitude acquires the maximum value, and the phase delay φ_x is just -90° [23]. It can be concluded from Equation (6) and (7) that with the difference between the drive force frequency w_d and drive resonant frequency w_x increasing, the vibration amplitude $|A_x|$ is smaller and the phase delay φ_x is far away from -90° in the working process. Therefore, the phase delay φ_x can be changed by adjusting the difference between w_d and w_x.

3. Impact and Theoretical Analysis of Circuit Phase Delay

Considering the inevitable manufacturing imperfections, the drive shaft (x direction) is not completely perpendicular to the sense shaft (y direction), damping and stiffness coupling of two modes cause in-phase force $F_I(t)$ and quadrature force $F_q(t)$. The Equation (2) can be described as Equation (8):

$$m_y\ddot{y} + c_y\dot{y} + k_y y + C_{xy}\dot{x} + k_{xy}x = F_y(t) - 2m_C\Omega_z\dot{x} \tag{8}$$

Preprints (www.preprints.org) | NOT PEER-REVIEWED | Posted: 13 April 2021 doi:10.20944/preprints202104.0346.v1

where C_{xy} is the coupling damping coefficient, k_{xy} is the coupling stiffness, take Equation (5) into Equation (8), the sense dynamics equation can be given as:

$$m_y\ddot{y} + c_y\dot{y} + k_y y = F_y(t) - 2m_C\Omega_z A_x w_d \sin(w_d t + \varphi_x)$$
$$- C_{xy}A_x w_d \sin(w_d t + \varphi_x) - k_{xy}A_x \cos(w_d t + \varphi_x) \quad (9)$$

According to the Coriolis effects, the direction of the acceleration is perpendicular to the direction of the input angular velocity and the driving vibration, hence, the in-phase force $F_I(t) = C_{xy}A_x w_d \sin(w_d t + \varphi_x)$ is proportional to the velocity, while the quadrature force $F_q(t) = k_{xy}A_x \cos(w_d t + \varphi_x)$ is proportional to the displacement of the drive mode.

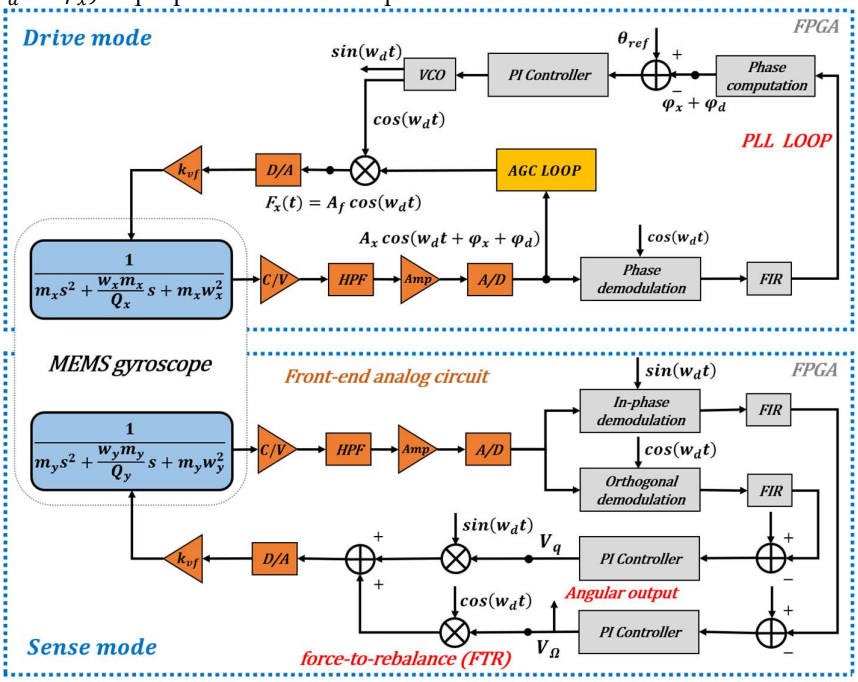

Figure 2. A schematic depiction for circuit phase delay of MEMS vibration gyroscopes.

According to [13], the noise of the system itself does not affect the calculation of the circuit phase delay, so the noise component in ZRO is ignored in the system phase analysis. Based on electrostatic drive and capacitance detection, the vibration gyroscope control system in this paper is mainly composed of front-end analog circuit, signal processing and loop control based on FPGA, as shown in Fig. 2. The front-end analog circuit is responsible for capacitor signal reading and conversion, signal amplification and filtering, analog-to-digital (A/D) and digital-to-analog (D/A) conversion. And the loop control system mainly consists of two parts: the drive mode control circuit composed of PLL and AGC loops keep the gyroscope vibration amplitude and frequency stable; a FTR closed-loop detection and quadrature error correction system is used to keep the sense mode relatively static and collect the angular velocity signal.

When the signal goes through D/A, A/D, C/V conversion, amplification, filtering and other modules of the control circuit, the circuit phase delay φ_d is inevitable. Without phase compensation (the reference value of the PLL is -90°), the existence of the PLL in the drive loop makes the difference between its input and output phase is -90°, therefore, the following phase relationship is satisfied:

$$\varphi_d = \varphi_{DA} + \varphi_{cv} + \varphi_{HPF} + \varphi_{AD} + \varphi_{oth} \quad (10)$$

$$\varphi_d + \varphi_x = -90° \quad (11)$$

where φ_{DA}, φ_{cv}, φ_{HPF}, φ_{AD} are the phase delay of DAC, C/V converter, High pass filter and ADC, respectively, and the φ_{ot} is the sum of other factors that introduce phase delay, such as V/F conversion, interface, etc. As seen from Equation (11), the existence of the circuit phase delay φ_d causes the drive phase delay $\varphi_x \neq -90°$. According to the previous analysis, shown in Equation (7),

Preprints (www.preprints.org) | NOT PEER-REVIEWED | Posted: 13 April 2021 doi:10.20944/preprints202104.0346.v1

it can be concluded that the circuit phase delay φ_d causes a frequency difference between drive force frequency w_d and drive resonant frequency w_x, and the gyroscope is not working in the resonance state. Next, the impact of circuit phase delay φ_d on the performance will be discussed deeply, and a real-time circuit phase delay measurement and compensation system is proposed.

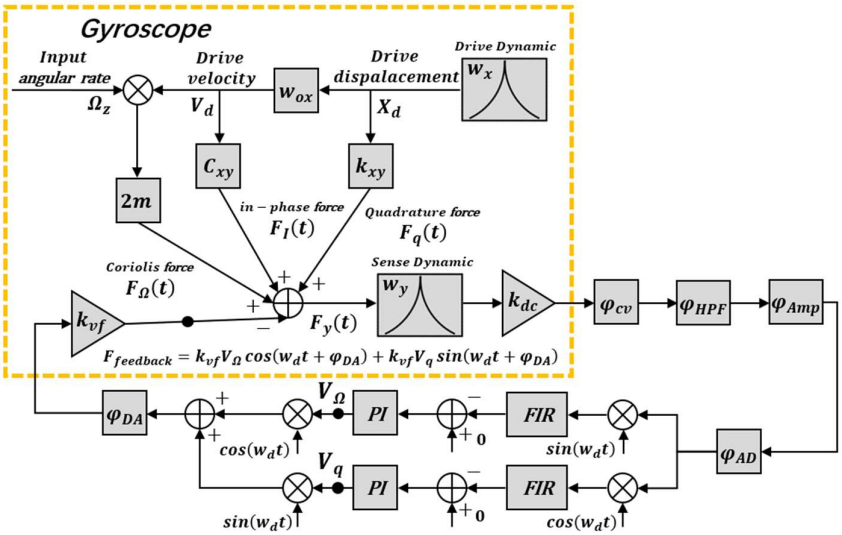

Figure 3. The phase system for the gyroscope sense model.

Considering the existence of circuit phase delay φ_d, the transient-response $x(t)$ of the driving direction changes, and the Equation (5) can be rewritten as:

$$x(t) = A_x \cos(w_d t + \varphi_x + \varphi_{DA}) \tag{12}$$

Under these circumstances, the sense dynamic Equation (9) is changed into:

$$\begin{aligned} m_y\ddot{y} + c_y\dot{y} + k_y y = F_y(t) - 2m_C\Omega_z A_x w_d \sin(w_d t + \varphi_x + \varphi_{DA}) \\ - C_{xy}A_x w_d \sin(w_d t + \varphi_x + \varphi_{DA}) - k_{xy}A_x \cos(w_d t + \varphi_x + \varphi_{DA}) \end{aligned} \tag{13}$$

The in-phase force $F_I(t) = C_{xy}A_x w_d \sin(w_d t + \varphi_x + \varphi_{DA})$, and the quadrature force $F_q(t) = k_{xy}A_x \cos(w_d t + \varphi_x + \varphi_{DA})$. As shown in Fig. 3, the FTR closed-loop detection and quadrature error correction control mechanism cause the resultant force exerted on the sense proof mass is nulled ($F_y(t) = 0$):

$$F_\Omega(t) + F_I(t) + F_q(t) = k_{vf}V_\Omega \cos(w_d t + \varphi_{DA}) + k_{vf}V_q \sin(w_d t + \varphi_{DA})\,. \tag{14}$$

$$\begin{aligned} 2m_C\Omega_z A_x w_d \sin(w_d t + \varphi_x + \varphi_{DA}) + C_{xy}A_x w_d \sin(w_d t + \varphi_x + \varphi_{DA}) + k_{xy}A_x \cos(w_d t + \varphi_x + \varphi_{DA}) \\ = k_{vf}V_\Omega \cos(w_d t + \varphi_{DA}) + k_{vf}V_q \sin(w_d t + \varphi_{DA}) \end{aligned}$$

Hence, the in-phase channel feedback output V_Ω and the quadrature channel feedback output V_q can be calculated:

$$\begin{cases} V_\Omega = \dfrac{[(2m_C\Omega_z A_x w_d + C_{xy}A_x w_d)\sin(\varphi_x) + k_{xy}A_x \cos(\varphi_x)]}{k_{vf}} \\ V_q = \dfrac{[(2m_C\Omega_z A_x w_d + C_{xy}A_x w_d)\cos(\varphi_x) - k_{xy}A_x \sin(\varphi_x)]}{k_{vf}} \end{cases} \tag{15}$$

From Equation (15), The phase relationship between the two channels of the sense mode depends on the drive phase delay φ_x. When the drive force frequency w_d is accurately locked to the drive resonant frequency w_x, the drive phase delay φ_x is -90°, the two channels are independent.

With the existence of circuit phase delay φ_d, the drive phase delay $\varphi_x \neq -90°$ according to Equation (11), the two channels are coupled to each other, a portion of the quadrature error fluctuation will be introduced into the angular velocity detection output, which seriously affects the performance of the vibration gyroscope. In this time, the output of the gyroscope at zero angular velocity input ($\Omega_z = 0$) is:

Preprints (www.preprints.org) | NOT PEER-REVIEWED | Posted: 13 April 2021 doi:10.20944/preprints202104.0346.v1

$$V_{\Omega} = \frac{[C_{xy}A_x w_d \sin(\varphi_x) + k_{xy}A_x \cos(\varphi_x)]}{k_{vf}} \tag{16}$$

Substituting Equation (11) into Equation (16), the relationship between the in-phase output and the circuit phase delay φ_d can be obtained as:

$$V_{\Omega=0} = \frac{[-C_{xy}A_x w_d \cos(\varphi_d) - k_{xy}A_x \sin(\varphi_d)]}{k_{vf}} \tag{17}$$

It can be seen from the above derivation that the existence of circuit phase delay φ_d leads to the coupling of in-phase and quadrature channel (IQ coupling), which introduce an uncontrollable low-frequency noise, leading to large drift in ZRO. Besides, the IQ coupling will reduce the scale factor of the system and affect the response to angular velocity of gyroscope, causing huge damage to the performance of gyroscope, such as BI and ARW. In order to eliminate the influence of circuit phase delay on the performances, it is essential to compensate the circuit phase delay φ_d.

4. Real-Time Circuit Phase Delay Correction System

A real-time circuit phase delay correction system is proposed in this section, which is based on the amplitude-frequency, phase-frequency characteristics of MEMS gyroscope and phase relationship of the whole control loop. It can be concluded from Equation (6) and (7) that when the excitation amplitude A_f is fixed, as the drive force frequency w_d is closer to the drive resonant frequency w_x, the vibration amplitude $|A_x|$ is larger and the phase delay of the drive mode is closer to -90°. When the w_d is equal to the w_x, the vibration amplitude $|A_x|$ acquires the maximum value, and the φ_x is just -90°.

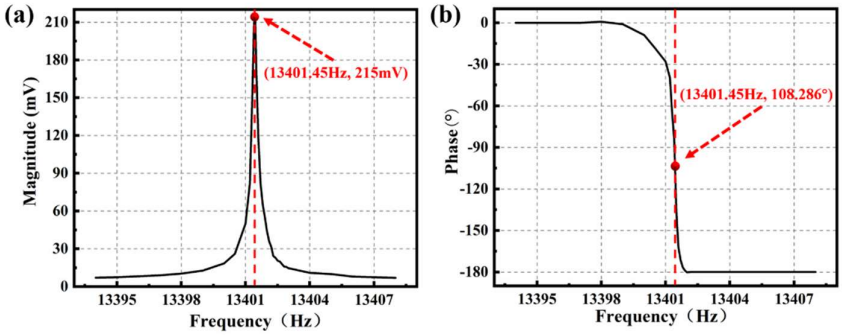

Figure 4. The (a) amplitude-frequency and (b) phase-frequency responses under open-loop frequency sweep.

In order to verify these characteristics of MEMS gyroscopes, an open-loop frequency sweep test on the front-end analog circuit is carried, as shown in [21]. The excitation signal with fixed amplitude (100 mV) and linearly increasing frequency (13394 Hz-13408 Hz; 0.05 Hz) was generated by FPGA programming, the amplitude and phase response under each excitation are automatically collected. As shown in Fig. 4 (a), when the frequency of excitation signal is 13401.45 Hz, the amplitude response of gyroscope reaches its maximum value, and the phase delay between excitation signal and output signal is 108.286° in this case, as shown in Fig. 4 (b). The experimental results show that it is feasible to study the phase delay of gyroscope with amplitude-frequency and phase-frequency characteristics. This one-time frequency sweep method is easy to operate and implement, the circuit phase delay φ_d of front-end analog circuit can be estimated to be about 108.286°—90° = 18.286° in this way. But the measured phase delay is the off-line phase delay of

Preprints (www.preprints.org) | NOT PEER-REVIEWED | Posted: 13 April 2021 doi:10.20944/preprints202104.0346.v1

gyroscope, it is unable to accurately measure the real phase delay in the working process, and the measured phase delay is not complete.

Based on the previous analysis, the drive force frequency w_d and the drive resonant frequency w_x can be gradually approached by compensating the circuit phase delay. When the phase delay φ_x is 90°, the vibration amplitude $|A_x|$ reaches the maximum value, and the compensated phase delay is the circuit phase delay of the whole circuit. Because of an AGC loop is adopted to makes vibration amplitude $|A_x|$ stability, the amplitude-frequency Equation (6) can be reduced to Equation (18). Therefore, when w_d and w_x are gradually approached by compensating the circuit phase delay, the excitation amplitude A_f becomes smaller, and the compensated phase delay is the real circuit phase delay φ_d until it reaches the minimum value.

$$A_f = |A_x| m_x \sqrt{(w_x^2 - w_d^2)^2 + w_x^2 w_d^2 / Q_x^2} \tag{18}$$

In order to measure and compensate the circuit phase delay in the working process, a real-time circuit phase delay correction system is proposed based on the previous analysis. The diagram of this real-time correction system is shown in Fig. 5, the detail process is described as follows.

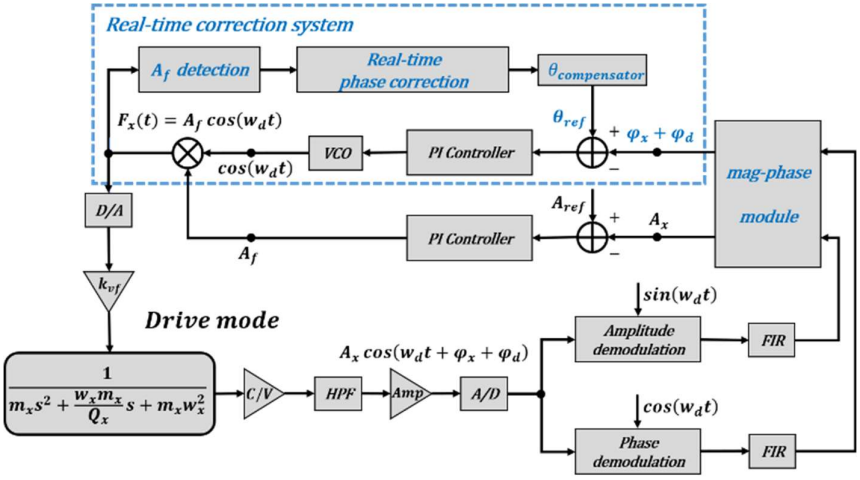

Figure 5. The diagram of real-time circuit phase delay correction system

(1) The gyroscope is in normal working condition: the PLL and AGC loops of the drive mode control circuit keep the gyroscope vibration amplitude and frequency stable, and a FTR closed-loop detection and quadrature error correction system is used to keep the sense mode relatively static and collect the angular velocity signal.

(2) The gyroscope starts up normally.

(3) When the gyroscope is stable, the circuit phase delay correction system starts to work, the change of excitation amplitude A_f is automatically detected to adjust the phase compensation value ($\theta_{compensator}$) and the reference value of PLL (θ_{ref}) is compensated gradually.

(4) Until the excitation amplitude A_f reaches the minimum value, the correction system tends to be stable. At this time, the phase compensation value ($\theta_{compensator}$) under the negative feedback balance is the real-time circuit phase delay in the working process.

(5) The measurement and compensation of the circuit phase delay φ_x are completed by the correction system, and the gyroscope is adjusted to the resonant working state.

Preprints (www.preprints.org) | NOT PEER-REVIEWED | Posted: 13 April 2021 doi:10.20944/preprints202104.0346.v1

A real-time circuit phase delay correction system is proposed, which can automatically measure and compensate for the circuit phase delay by detecting the excitation amplitude A_f and adjusting the reference value of PLL (θ_{ref}). When the circuit phase delay is compensated, the phase delay φ_x is just -90° and the drive force frequency w_d is exactly equal to the drive resonant frequency w_x.

5. Experimental results and analysis

Self-developed shock resistant vibration gyroscopes are adopted in this paper. A non-decoupled structure is designed to improve the impact resistance (about 100000 g, which is crucial in tactical applications) of gyroscopes. To achieve large vibration amplitude, the silicon wafers prefabricated with sensing structures were anodically bonded under high vacuum pressure (about 0.8 mbar) at wafer level [24]. Photograph of the Wafer-Level-Package (WLP) capacitive vibration gyroscopes is shown in Fig. 6, the size of the gyroscopes is only 3 mm × 3 mm, custom-made packages with metal lids are used to avoid the electrostatic charging caused by external sources [25]. The designed real-time circuit phase delay correction system is tested on these Self-developed shock resistant vibration gyroscopes. The circuit control system is mainly composed of analog front-end circuit and FPGA, and the USART is used for data acquisition at a 1KHz sampling rate.

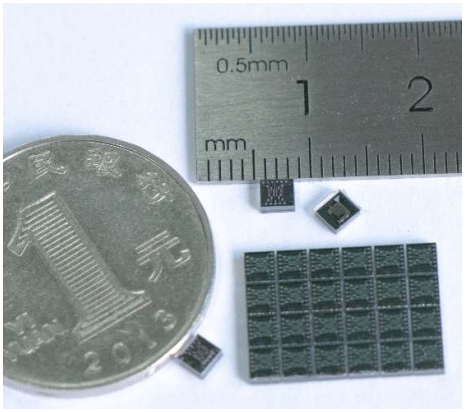

Figure 6. Photograph of Wafer-Level-Package capacitive vibration gyroscope.

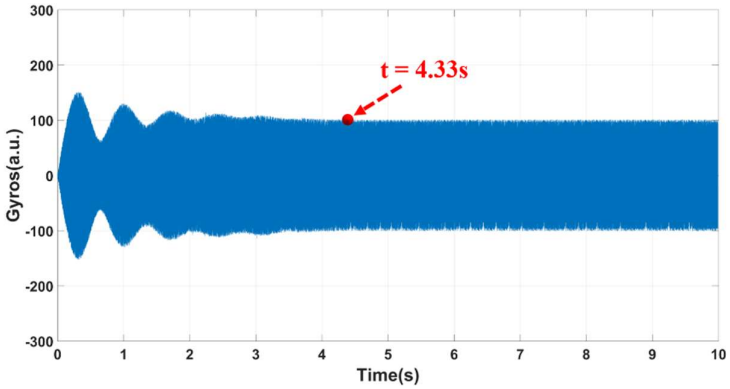

Figure 7. A diagram for the start-up process of MEMS gyroscopes.

In order to effectively measure and compensate the circuit phase delay in the working process, the stability time of MEMS gyroscope control loop is measured to avoid the interference between the real-time circuit phase delay correction system and the start-up process. The test results are shown in the Fig. 7, it can be seen that the turn on time is about 4.33 s. Therefore, a 5 s delay is set in

Preprints (www.preprints.org) | NOT PEER-REVIEWED | Posted: 13 April 2021 doi:10.20944/preprints202104.0346.v1

the correction system to ensure the normal operation of the MEMS gyroscope and effectively measure and compensate the circuit phase delay in the working process.

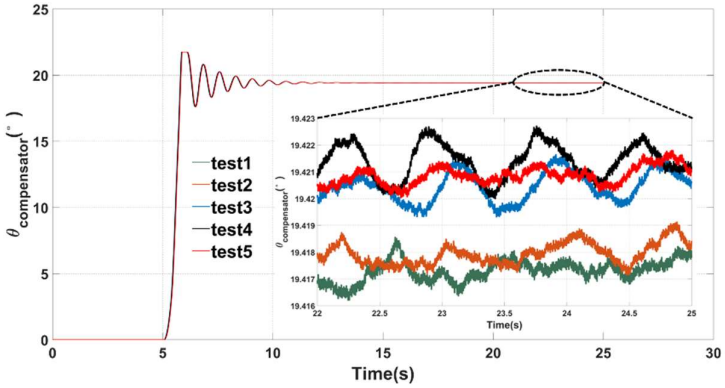

Figure 8. Test results of the real-time circuit phase delay correction system.

After the MEMS gyroscope works normally, the real-time circuit phase delay correction system starts to work, and the reference value of PLL is automatically adjusted by collecting the change of the excitation amplitude A_f until a negative feedback equilibrium is reaching. In order to verify the effectiveness of the correction system, five repeated experiments are carried out. The test results are shown in Fig. 8, this correction system has excellent repeatability and stability, which can effectively measure and compensate the real-time circuit phase delay within 10 seconds, the measured circuit phase delay is about 19.419 ± 0.004° in the working process.

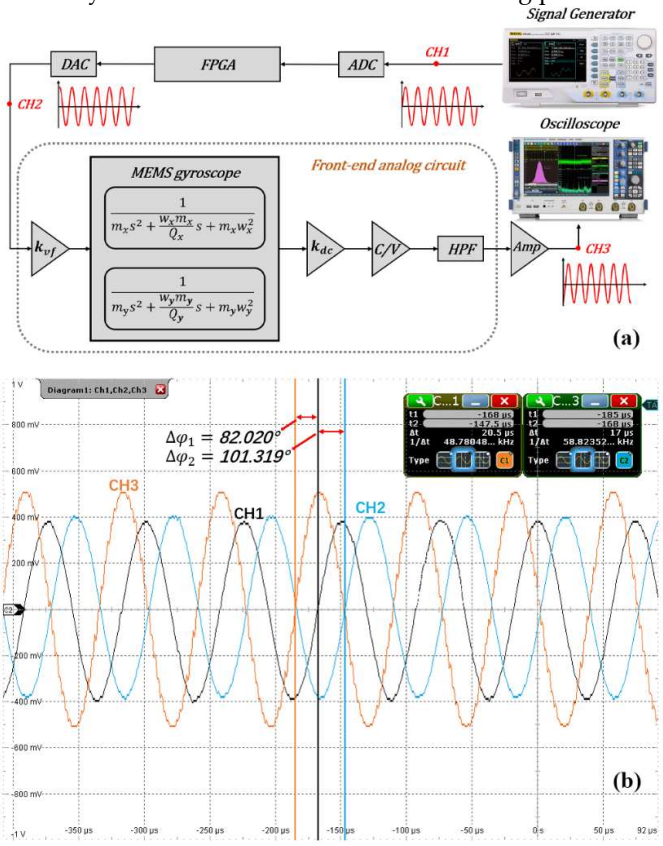

Figure 9. (a) The schematic diagram and (b) the test results of one-time circuit phase delay measurement.

To investigate the feasibility of this real-time correction system, the circuit phase delay of the system was verified by the one-time measurement method as shown in Fig. 9 (a). The excitation

Preprints (www.preprints.org) | NOT PEER-REVIEWED | Posted: 13 April 2021 doi:10.20944/preprints202104.0346.v1

frequency obtained from the open-loop frequency sweep test in section 4, an excitation signal (CH1) with a frequency of 13401.45 Hz and an amplitude of 400 mV is generated by the signal generator (RIGOL DG4202). This signal is collected by ADC and processed by FPGA, and then passes through DAC. After DC isolation, the MEMS gyroscope vibration, and the vibration output signal through CV conversion, filtering and amplification. An oscilloscope (R&S ®RTO2000) is used to detect the phase change of the excitation signal. Fig. 9 (b) shows the test results of three channels (CH1, CH2 and CH3), the circuit phase delay of signal processing modules (from ADC to DAC) is $90°-82.020°=7.98°$, and the circuit phase delay of analog front-end circuit is $101.319°-90°=11.319°$. By calculation, the total circuit phase delay of one-time measurement method is $7.98°+11.319°=19.299°$. Comparing with the real-time circuit phase delay correction system, the deviation is only about 1%, which verify that this correction system can accurately and effectively measure the circuit phase delay.

To measure the scale factor before and after phase delay compensation, the MEMS gyroscope and circuit system are placed on the angular velocity table (TBL-S1101-AT03). The continuous angular velocity rates, such as 0°/s, ±0.5°/s, ±1°/s, ±5°/s, ±10°/s, ±50°/s, ±100°/s, ±200°/s and so on are applied during the test, each sampling points is collected for 1 minute and the average value is taken as the corresponding angular rate output. As shown in Fig. 10, the full-scale range of the gyroscopes is over 1800°/s, which has a high-rate resolution as low as 0.1°/s. Without phase compensation, the scale factor is 1.203 mV/(°/s) with a nonlinearity of 2600 ppm, and the scale factor is 1.303 mV/(°/s) with a nonlinearity of 660 ppm under one-time phase delay compensation. The scale factor is 1.345 mV/(°/s) with a nonlinearity of 255 ppm under real-time phase delay compensation, which is about 10.2 times improvement on the nonlinearity. Comparing with no phase delay compensation, the phase delay correction system can effectively improve the angular velocity response of gyroscopes by reducing the IQ coupling, and the nonlinearity of the scale factor is significantly improved.

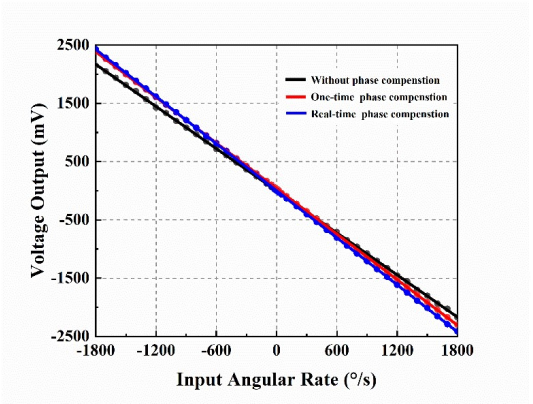

Figure 10. Test of full scale and nonlinearity of the vibration gyroscope.

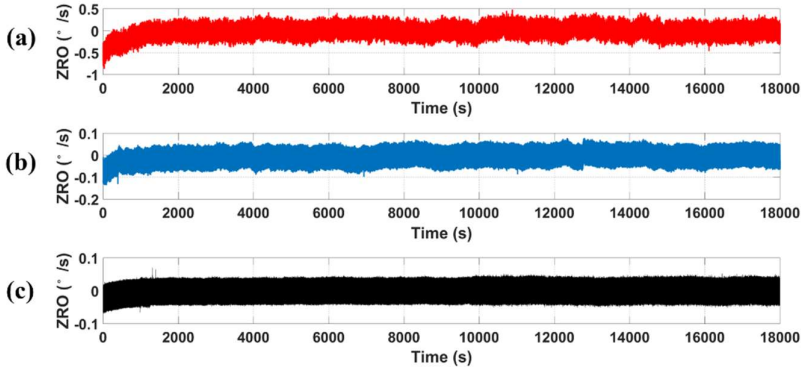

Figure 11. ZRO acquired of (a) without; (b) one-time and (c) real-time phase delay compensation at room temperature.

Preprints (www.preprints.org) | NOT PEER-REVIEWED | Posted: 13 April 2021 doi:10.20944/preprints202104.0346.v1

Fig. 11 shows the measured ZRO at room temperature, the output angular rate is recorded at a 1 kHz sample rate for 5 h. Without phase delay compensation, the reference value θ_{ref} of the PLL is manually configured as -90°, and the θ_{ref} of one-time phase delay compensation adopts the value -109.299° obtained from the previous one-time phase delay measurement. As shown in Fig. 11 (a), the variation of ZRO is about 0.812°/s without phase delay compensation, and the ZRO of one-time phase delay compensation is 0.14°/s shown in Fig. 11 (b). The ZRO is improved about 8.55 times to 0.095°/s under the real-time phase delay compensation shown in Fig. 11 (c). Experimental results show that the real-time circuit phase delay correction system can effectively reduce the fluctuation of output angular by eliminating the unwanted IQ coupling and reduce the effect of quadrature error on ZRO.

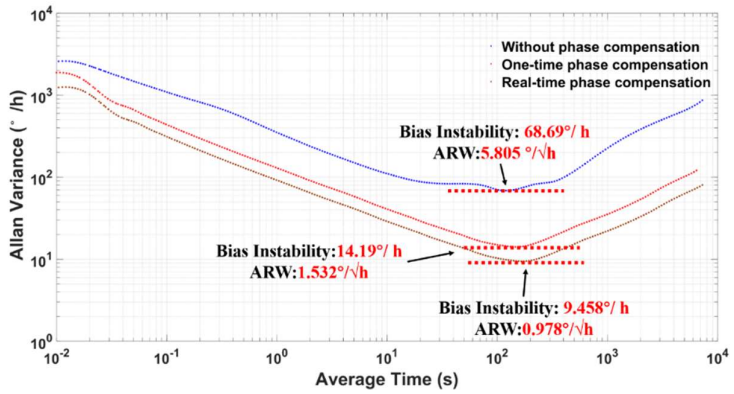

Figure 12. Allan variance plot at room temperature.

The Allan variance plot is obtained from the ZRO data collected previous and shown in Fig. 12. It shows that the measured Bias instability is 68.69°/h and the ARW is 5.805°/√h without phase delay compensation. Besides, the Bias instability is 14.19°/h and the ARW is 1.532°/√h under one-time phase delay compensation. Comparing with no phase delay compensation, the Bias instability is increased by 7.26 times to 9.458°/h and the ARW is increased by 5.94 times to 0.978°/√h respectively in the condition of the real-time phase delay compensation. The Allan variance results prove that this phase delay correction system is effective in improving the BI and ARW performance of MEMS gyroscopes by eliminating the IQ coupling.

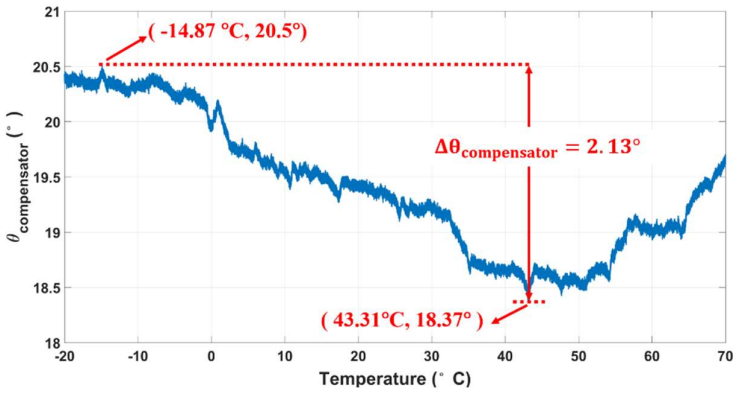

Figure 13. Measured circuit phase delay respect to temperature.

The performance of MEMS gyroscope is directly affected by the change of ambient temperature, besides, the phase delay of the amplifier, resistor, capacitor and processor modules in the circuit is affected by temperature. To verify the compensation effect of the real-time circuit phase delay correction system in this case, the MEMS gyroscope and circuit system are placed in (HK-GDW-80), and the temperature measurement range is from -20°C to 70°C. As shown in Fig. 13, the circuit phase delay decreases first and then increases with the change of temperature, the maximum phase variation is about 2.13°. The variation curves of ZRO without phase compensation are shown in Fig.

Preprints (www.preprints.org) | NOT PEER-REVIEWED | Posted: 13 April 2021 doi:10.20944/preprints202104.0346.v1

14 (a), the ZRO gradually rises with the increasing of temperature, and reaches 3.642°/s at 70°C. However, the change trend of ZRO gradually slow down with real-time phase compensation and the maximum variation is only 0.302°/s shown in Fig. 14 (b). The temperature coefficient (TCO) of ZRO reduces from 0.04°/s/°C to 0.0034°/s/°C and increased about 12.1 times. Experimental results show that the real-time circuit phase delay correction system can effectively track the variation of circuit phase delay with the change of environment temperature, which realizes the precise measurement and compensation of circuit phase delay. Besides, this correction system is robust against the temperature change, and can effectively reduce the influence of temperature change on the performance of MEMS gyroscope.

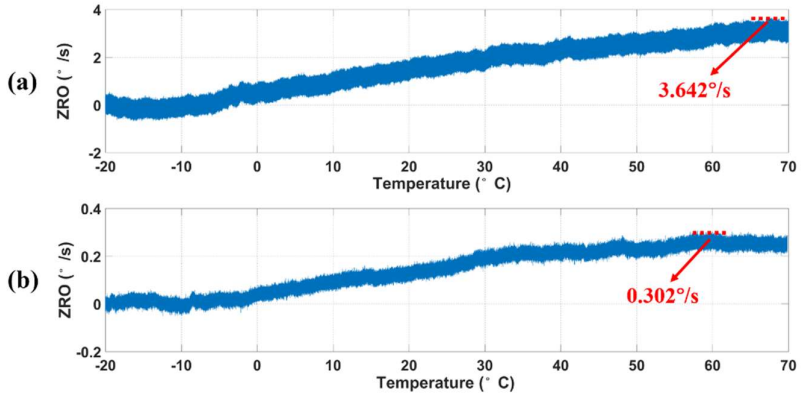

Figure 14. The measured ZRO (a) without and (b) with phase delay compensation respect to temperature.

Table 1. The performance of MEMS gyroscope with and without phase delay compensation.

	Without phase compensation	One-time phase compensation	Real-time phase compensation	Improve
Zero rate output (°/s)	0.812	0.14	0.095	8.55
Scale factor (mV/(°/s))	1.203	1.303	1.345	1.12
Nonlinearity (ppm/°C)	2600	660	255	10.2
Bias instability (°/h)	68.69	14.19	9.458	7.26
Angle random walk (°/√h)	5.805	1.532	0.978	5.94
TCO of ZRO (°/s/°C)	0.04	---	0.0034	12.1

Table 1. shows the summary of the measured performance with and without phase compensation. The real-time circuit phase delay correction system can effectively eliminate the unwanted IQ coupling and reduce the effect of quadrature error on ZRO through accurately measure and compensate the circuit phase delay in real time. Ultimately, the ZRO, the Scale factor, the BI, the ARW and the TCO of ZRO are significantly improved.

7. Conclusions

In summary, a real-time circuit phase delay correction system is proposed to automatically measure and compensate the circuit phase delay for MEMS vibratory gyroscopes. The effect of circuit phase delay on IQ coupling and ZRO is analyzed under FTR closed-loop detection and quadrature error correction system. By accurately measuring and compensating the real-time circuit phase delay, the correction system can effectively eliminate the unwanted IQ coupling and greatly improve the performance of MEMS gyroscope. This correction system achieves a decreased ZRO down to 0.095°/s, a small ARW of 0.978°/√h, and a low BI of 9.458°/h together with a scale factor nonlinearity of 255 ppm at room temperature. It is shown that the correction system is robust against the temperature change and the thermal drifts of ZRO is reduced to 0.0034°/s/°C. Our work presents a novel method to measure and compensate the circuit phase delay in real time, which may promote the evolution of high-performance MEMS gyroscopes for potential applications.

Author Contributions: Conceptualization, Pengfei Xu; Data curation, Pengfei Xu, Zhenyu Wei, Zhiyu Guo and Fuhua Yang; Resources, Guowei Han, Chaowei Si and Jin Ning; Software, Pengfei Xu; Supervision, Guowei Han, Chaowei Si, Jin Ning and Fuhua Yang; Validation, Pengfei Xu and Lu Jia; Writing – original draft, Pengfei Xu; Writing – review & editing, Guowei Han, Chaowei Si, Jin Ning and Fuhua Yang.

Funding: This work is supported by the National Key R&D Program of China (No.2018YFF01010500).

Conflicts of Interest: The authors declare no conflict of interest.

References

1. Marx M, Dorigo D D, Nessler S, et al. 9.4 A 27μW 0.06mm 2 background resonance frequency tuning circuit based on noise observation for a 1.71mW CT-ΔΣ MEMS gyroscope readout system with 0.9°/h bias instability[C] Solid-state Circuits Conference. IEEE, 2017.
2. Li C, Yang B, X Guo, et al. A Digital Calibration Technique of MEMS Gyroscope for Closed-Loop Mode-Matching Control[J]. Micromachines, 2019, 10(8).
3. Zhanshe G, Fucheng C, Boyu L, et al. Research development of silicon MEMS gyroscopes: a review[J]. Microsystem Technologies, 2015, 21(10):2053-2066.
4. Cui J, Zhao Q, Yan G. Effective bias warm-up time reduction for MEMS gyroscopes based on active suppression of the coupling stiffness[J]. Microsystems & Nanoengineering, 2019, 5(1):18-.
5. Lutwak R. Micro-technology for positioning, navigation, and timing towards PNT everywhere and always[C] 2014 International Symposium on Inertial Sensors and Systems (ISISS). IEEE, 2014.
6. Biswas A, VS Pawar, Menon P K, et al. Influence of fabrication tolerances on performance characteristics of a MEMS gyroscope[J]. Microsystem Technologies, 2020(12).
7. Olaf D, Georg D, Stefan K, et al. MEMS and FOG Technologies for Tactical and Navigation Grade Inertial Sensors—Recent Improvements and Comparison[J]. Sensors (Basel, Switzerland), 2017, 17(3).
8. Lavrik N V, Datskos P G. Optically read Coriolis vibratory gyroscope based on a silicon tuning fork[J]. Microsystems & Nanoengineering.
9. Schofield A, Trusov A, Shkel A. Micromachined gyroscopes with 2-DOF sense modes allowing interchangeable robust and precision operation[J]. 2013.
10. Painter, C. C, Shkel, et al. Active structural error suppression in MEMS vibratory rate integrating gyroscopes[J]. Sensors Journal, IEEE, 2003, 3(5):595-606.
11. Zhao Y, Jian Z, Xi W, et al. A Sub-0.1°/h Bias-Instability Split-Mode MEMS Gyroscope With CMOS Readout Circuit[J]. IEEE Journal of Solid State Circuits, 2018:1-15.
12. Ezekwe C D, Geiger W, Ohms T. 27.3 A 3-axis open-loop gyroscope with demodulation phase error correction[C] 2015 IEEE International Solid-State Circuits Conference - (ISSCC) Digest of Technical Papers. IEEE, 2015.
13. Feng, Bu, Shuwen, et al. Effect of circuit phase delay on bias stability of MEMS gyroscope under force rebalance detection and self-compensation method[J]. Journal of Micromechanics & Microengineering, 2019, 29(9):95002-95002.
14. Xing L, Xiong Z, Liu J Y, et al. Offline Calibration for MEMS Gyroscope G-sensitivity Error Coefficients Based on the Newton Iteration and Least Square Methods[J]. Journal of Navigation, 2017, 71(2):1-19.
15. Zhao W, Yang H, Liu F, et al. High sensitivity rate-integrating hemispherical resonator gyroscope with dead area compensation for damping asymmetry[J]. Scientific Reports, 2021, 11(1):2195.
16. Tatar E. Quadrature-Error Compensation and Corresponding Effects on the Performance of Fully Decoupled MEMS Gyroscopes[J]. Journal of Microelectromechanical Systems, 2012, 21(3):656-667.
17. Chen F, Gu J, Salimi P, et al. Self-Clocking Electro-Mechanical Sigma-Delta Modulator Quadrature Error Cancellation for MEMS Gyroscope[C] The 32nd IEEE International Conference on Micro Electro Mechanical Systems (MEMS 2019). IEEE, 2019.
18. Thiyagarajan V, Kabilan A P, Madheswaran M, et al. Adaptive IQ mismatch cancellation for quadrature if receivers[C] Proceedings of the 4th WSEAS International Conference on Signal Processing, Robotics and Automation. 2005.
19. Gu H, Su W, Zhao B, et al. A Design Methodology of Digital Control System for MEMS Gyroscope Based on Multi-Objective Parameter Optimization[J]. Micromachines, 2020, 11(1).

20. Omar A, Elshennawy A, Abdelazim M, et al. Analyzing the Impact of Phase Errors in Quadrature Cancellation Techniques for MEMS Capacitive Gyroscopes[C] 2018 IEEE SENSORS. IEEE, 2018.
21. Wei M, Liu S, Lin Y, et al. One-time frequency sweep to eliminate IQ coupling in MEMS vibratory gyroscopes[C] 2016 IEEE International Conference on Manipulation, Manufacturing and Measurement on the Nanoscale (3M-NANO). IEEE, 2017.
22. Bai B, Li C, Zhao Y. Development of V-Shaped Beam on the Shock Resistance and Driving Frequency of Micro Quartz Tuning Forks Resonant Gyroscope[J]. Micromachines, 2020, 11(11):1012.
23. Wang X, Li H, Xia G, et al. Research and experiment on the drive frequency control of the MEMS gyroscope[C] Second International Conference on Mechanic Automation & Control Engineering. IEEE, 2011.
24. Zhang M, Yang J, He Y, et al. Research on a 3D Encapsulation Technique for Capacitive MEMS Sensors Based on Through Silicon Via[J]. Sensors, 2018, 19(1).
25. Lapadatu D, Blixhavn B, Holm R, et al. SAR500 - A high-precision high-stability butterfly gyroscope with north seeking capability[C] Position Location & Navigation Symposium. IEEE, 2010.